Catalysis Science & Technology

ROYAL SOCIETY OF CHEMISTRY

PAPER

View Article Online
View Journal



Cite this: DOI: 10.1039/d5cy01486g

# Ru/$CeO_2$ catalysts for supercritical water gasification of glycerol: stability, activity, and coke hydrothermal oxidation

Tomasz Kondratowicz, †[a] Aurélien Quenet,†[ab] Xujun Li,[a] Andrea Testino, [ac] Oliver Kröcher, [ab] Frédéric Vogel [ad] and David Baudouin *[a]

Cerium oxide ($CeO_2$) was investigated as a support for Ru nanoparticles in the continuous supercritical water gasification (SCWG) of glycerol as a model biomass compound. The stability of pure $CeO_2$ under reductive SCW conditions was first assessed in both batch and continuous modes. In batch, $CeO_2$ readily underwent phase transformation to $CeCO_3OH$, implying reduction of $Ce^{4+}$ to $Ce^{3+}$, leading to severe loss of surface area. The formation of $CeCO_3OH$ was completely prevented in continuous flow due to the flushing of $CO_2$ and reductive compounds before cooling down to a temperature thermodynamically favouring $CeCO_3OH$. Although pristine $CeO_2$ showed low activity in SCWG, thermal treatment strongly influenced product distribution, with CO disappearing in favour of $C_3H_8$ after a reductive pretreatment. When Ru nanoparticles were supported on thermally stabilized $CeO_2$ (calcined at 700–900 °C, 0.11–1.00 wt% Ru), the catalysts displayed high efficiency in SCWG of glycerol, yielding $CO_2$, $CH_4$, and $H_2$ as the main products. These Ru/$CeO_2$ catalysts achieved apparent conversion rates up to three times higher than a commercial 5 wt% Ru/AC benchmark, while maintaining similar selectivity trends. Both Ru/$CeO_2$ and carbon-based catalysts exhibited similar decreasing activity trends under operation. Post-reaction analysis revealed some carbon deposition on Ru/$CeO_2$, likely the main cause of the observed loss of activity, which could be effectively removed either by thermal oxidation in air at 300 °C or by *in situ* hydrothermal oxidation with $H_2O_2$ at 110 °C. Overall, Ru/$CeO_2$ emerges as a durable and regenerable alternative to Ru/carbon for SCWG applications.

Received 5th December 2025,
Accepted 5th May 2026

DOI: 10.1039/d5cy01486g

rsc.li/catalysis



## Introduction

Climate change, driven by anthropogenic greenhouse gas (GHG) emissions, is intensifying extreme weather events, threatening ecosystems, agriculture, and economies.[1,2] The Paris agreement seeks to limit global warming below 2 °C, ideally 1.5 °C, requiring rapid GHG reduction.[3] Some sectors, such as transportation and heavy industry, are hard to decarbonise and rely heavily on fossil fuels,[4] necessitating a shift to renewable chemical energy carriers. Currently contributing to 9.8% of the global energy supply,[5] biomass offers a promising alternative, enabling carbon-neutral energy while valorising organic waste streams. However, traditional biomass utilization faces hurdles, including low energy density, land-use conflicts, and high water content.[6,7]

Hydrothermal gasification (HTG), particularly supercritical water gasification (SCWG), efficiently converts wet biomass into methane or hydrogen-rich gas under high-temperature, high-pressure conditions.[8–14] Unlike conventional methods, SCWG eliminates the need for drying the feedstock, making it ideal for processing sewage sludge, wet agricultural residues, municipal waste, and algae. By enhancing waste valorisation and clean energy production, SCWG can help reduce society's dependence on fossil fuels.[14] SCWG converts wet biomass into gas through various competing reactions, with composition dependent on process parameters and catalyst used. Operating at 380–700 °C and pressures above 221 bars, SCWG gasifies diverse organic feedstocks[8–12] and separates inorganic components due to their low solubility in supercritical water (SCW).[15–17] Catalytic SCWG (cSCWG), typically operated at 374–450 °C, yields a methane-rich gas through the use of Ru- or Ni-based catalysts while allowing high conversion rates.[9,10,18]

[a] *PSI Center for Energy and Environmental Sciences, Paul Scherrer Institute (PSI), 5232 Villigen PSI, Switzerland. E-mail: david.baudouin@psi.ch*
[b] *Institute of Chemical Sciences and Engineering, École Polytechnique Fédérale de Lausanne (EPFL), 1015 Lausanne, Switzerland*
[c] *Institute of Materials, École Polytechnique Fédérale de Lausanne (EPFL), 1015 Lausanne, Switzerland*
[d] *University of Applied Sciences Northwestern Switzerland (FHNW), School of Engineering and Environment, 5210 Windisch, Switzerland*
† These authors contributed equally to the research and are to be considered co first authors.

State-of-the-art catalysts for cSCWG are ruthenium nanoparticles on carbon-based supports, typically activated carbon.[10,19,20] Nickel, despite its lower price, exhibited poor stability under these conditions, suffering from sintering or leaching.[21–24] Ru nanoparticles supported on carbon nanofiber (CNF) showed outstanding activity, and above 1.5 nm diameter, the particle size showed negligible impact on the intrinsic activity of Ru, *i.e.* no effect on turnover frequency (TOF).[25] Ru particles below 1.5 nm diameter proved intrinsically more active but also suffered from severe deactivation, as opposed to larger particles. Interestingly, a clear correlation between TOF and Ru surface loading was found.[25] These catalysts show, however, fast deactivation in the first hours of testing due to some particle size growth ("sintering") and coking, with an exponential decay stabilizing towards a steady-state TOF. The size of supported Ru particles have been shown to always stabilise to the same range of 2–3 nm for CNF, AC, or $ZrO_2$, even at high loadings, after continuous cSCWG tests using model feedstock.[20,25] Aside of catalyst poisoning, coking remains the main cause of deactivation. Regeneration of Ru/AC catalysts is possible *via* mild hydrothermal oxidation with $H_2O_2$ to remove sulphur and/or coke, but it is still challenging because selective coke removal inevitably causes partial damage to the carbon support.[26–28] Ru remains the best active phase for cSCWG in all aspects, but its high cost represents a non-negligible expenditure. The yearly OPEX linked to the catalyst regeneration, its partial replacement and that of the sulfur scavenger represents *ca.* 8% of the CAPEX of a 3 t $h^{-1}$ plant for wet biomass or wastes such as sewage sludge or digestates.[29] In order to reduce this cost, beyond its high activity, a catalyst with a high stability and regenerability is of utmost importance.

Catalysts using oxides as support have so far systematically shown poor TOF and/or poor stability in continuous-flow SCWG, when compared to carbon-supported catalysts.[10,20,30,31] Stable oxides typically have low specific surface area under SCWG conditions (reducing conditions), and they are significantly surpassed by carbon with its high surface area, good stability and low cost.[31] Besides these advantages, Ru nanoparticles show much higher performance when supported on carbon, compared to any oxide investigated so far.

$CeO_2$ is known for its oxygen storage capacity (OSC) allowing oxygen donation to supported metal nanoparticles, which limits coke formation.[32] The operating temperature of OSC is highly dependent on the heat treatment conditions, morphology, and porosity of $CeO_2$, but is typically in the range of 300–500 °C.[33] Several recent studies have shown a clear link between the OSC of the support and the catalyst activity when $CeO_2$-based supported nanoparticles were used, for instance in the water gas shift reaction (WGS)[34–38] or reverse WGS.[39] The presence of noble metal nanoparticles such as platinum was proved to enhance the reducibility of a $CeO_2$-based support.[40] The OSC of $CeO_2$ can be tuned (increased or decreased) by adding to it various elements ("doping"), such as Zr, La, or Fe. The choice of the dopant was found to severely affect the selectivity of a catalyst,[41] and to influence adsorption and activation of gases on the support.[42]

The low solubility of cerium oxide in pure SCW was reported from thermodynamic calculations, and its potential stability was experimentally confirmed,[21,22] but the nature of the stable phase strongly depends on pH, oxygen fugacity and temperature.[21] While physical stability of $CeO_2$ nanoparticles under reductive supercritical water was proven,[43] the partial reduction of $Ce^{4+}$ to the $Ce^{3+}$ phase (formation of $CeCO_3OH$), has been reported[44] and is expected to be the cause of a major loss of specific surface area and porosity.

This paper aims at exploring the potential of $CeO_2$ as a support for Ru nanoparticles for the continuous cSCWG. First, the stability of $CeO_2$ under reductive cSCWG conditions was investigated, both in batch and continuous mode. Then, the most stable oxides were used to prepare Ru/$CeO_2$ catalysts with different loadings, in a similar range as those determined as optimal for CNF as a support.[25] Finally, their performances were then evaluated in the cSCWG of glycerol and compared with the benchmark catalysts Ru/CNF and Ru/AC. Coke deposits formed on the spent catalyst were studied and the regeneration capability of such class of catalysts was assessed as well.

## Results and discussion

### Ceria stability in SCWG: batch *vs.* continuous

The X-ray powder diffraction (XRD) patterns recorded for the pristine $CeO_2$ sample and the ones after the performed SCWG of glycerol (batch and continuous flow experiments) at 430 °C and 270 bar are shown in Fig. 1. The raw $CeO_2$ possesses a set of diffraction lines at $2\theta$ = 28.5°, 33.1°, 47.5°, 56.3°, 59.1°, 69.4°, 76.6° and 79.1°, assigned to the (111), (200), (220), (311), (222), (400), (311), (420) and (113) planes typical of pure $CeO_2$ in the face-centred cubic fluorite structure with Fm-3m space group (JCPDS 34-0394).[45] After

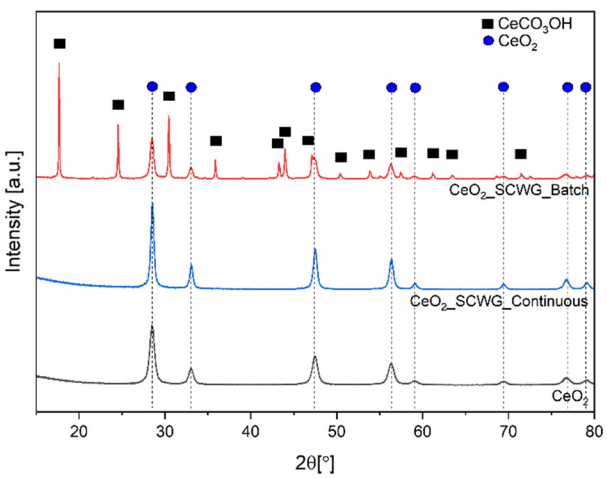


Fig. 1 XRD patterns of $CeO_2$ before and after SCWG batch and continuous experiments.

**Table 1** Textural properties of $CeO_2$ after various treatments

| Sample | SCW/SCWG conditions | $S_{BET}$ [$m^2$ $g^{-1}$] | $V_{total}$ [$cm^3$ $g^{-1}$] | Crystallite size[a] [nm] |
|---|---|---|---|---|
| $CeO_2$ | N/A | 53 | 0.098 | 18 |
| $CeO_2$_SCW_batch | $H_2O$, 30 min, 430 °C, 270 bar | 27 | 0.095 | 30 |
| $CeO_2$_SCWG_batch | 10 wt% glycerol, 30 min, 430 °C, 270 bar[b] | 7.0 | 0.028 | 30 |
| $CeO_2$_SCWG_batch_pH = 7 | 10 wt% glycerol in phosphate buffer, 30 min, 430 °C, 270 bar | 16 | 0.050 | 28 |
| $CeO_2$_SCWG_continuous | 10 wt% glycerol, 15 g $min^{-1}$, 3 h, 430 °C, 270 bar | 20 | 0.095 | 31 |

[a] Crystallite size of $CeO_2$ evaluated *via* Rietveld refinement. [b] Note that the mechanical strength (not measured) of the pellet after the test without buffering has significantly increased, as evidenced during crushing of the pellets prior to XRD analysis.

being exposed to pure supercritical water for 30 min (in the batch reactor), the material did not suffer from any loss of physical integrity nor from any significant phase evolution. However, an increase of crystal size from 18 to 30 nm was observed resulting in a decrease in surface area from 53 to 17 $m^2$ $g^{-1}$ (Fig. S1 and Table 1).

The oxygen fugacity of the reaction media greatly impacts the stability of the cerium phases under the conditions applied,[21] therefore tests with 10 wt% glycerol in water were also performed. During these experiments under reductive conditions, the $CeO_2$ sample evolved rapidly, and already after 30 min, a new highly crystalline phase appeared, aside the cubic fluorite $CeO_2$ structure. The most intense set of reflections of this new phase were at $2\theta$ = 17.7°, 24.5°, 30.4°, 35.9°, 43.3°, 44.0°, 47.1°, 53.8°, 57.4° and 61.2°, which can be assigned to the (002), (030), (032), (004), (330), (034), (332), (062), (334) and (036) planes, respectively, typical for the $CeCO_3OH$ phase crystalised in the hexagonal space group P-6 (ICSD 238537).[46] The formation of this $CeCO_3OH$ phase involves the reduction of $Ce^{4+}$ to $Ce^{3+}$. Detailed phase analysis using Rietveld refinement of the XRD data was performed with GSAS-II software (Fig. S2 and Table S1) and good agreement was obtained for the two-phase model ($CeO_2$ and $CeCO_3OH$). Based on performed calculations, this sample consists of 44 wt% $CeO_2$ and 56 wt% $CeCO_3OH$. In parallel to this partial change of phase, a significant reduction in porosity of the spent material was observed (Table 1). The BET surface area ($S_{BET}$) and total pore volume ($V_{total}$) obtained from $N_2$ physisorption analysis dropped drastically from 53 to 7.0 $m^2$ $g^{-1}$ and 0.098 to 0.028 $cm^3$ $g^{-1}$, respectively. The phase change was also associated with a significant increase of the mechanical strength (not measured) of the pellet as evidenced during crushing of the pellets prior to powder XRD analysis. The observed phase transformation is consistent with the results from Guan *et al.*, who also noted a phase transformation of ceria (support of Ru phase) after SCWG of phenol in a batch reactor.[44] The formation of water-soluble $Ce^{3+}$ species ($CeO^+$, $CeOH^{2+}$) have been predicted by Jocz *et al.* at concentrations higher than ≈1 mmol $kg^{-1}$ to occur under reductive supercritical water conditions below pH 6 at 380 °C and 300 bar. This pH limit (recalculated under process conditions) declines with increasing temperature and decreasing pressure, *e.g.* pH 4 at 450 °C and 300 bar or 380 °C and 220 bar.[21] During the gasification of glycerol under batch conditions, the pH of the solution decreased from 7 to 4. To evaluate the effect of pH on the formation of this phase, an attempt was made to stabilise $CeO_2$ by controlling the pH of the glycerol feed solution. For this purpose, a phosphate buffer was added. Note that despite of this buffer, the pH decreased from 7 to 6 (measured before and after the test at ambient conditions) after the SCWG experiment under analogous conditions. The post-test XRD analysis (Fig. S3) shows that the increase of the pH limited the appearance of the undesired phase but did not prevent it (sample composition: 70 wt% of $CeO_2$ and 30 wt% of $CeCO_3OH$). The control of the pH also led to a smaller decrease in porosity compared to the experiment conducted without pH stabilization ($S_{BET}$ = 16 *vs.* 7.0 $m^2$ $g^{-1}$ and $V_{total}$ = 0.050 *vs.* 0.028 $cm^3$ $g^{-1}$). This supports the hypothesis that a dissolution-recrystallization process is favoured at lower pH, inducing coarsening ("sintering") of $CeO_2$ and resulting in higher concentration of $Ce^{3+}$.[21]

Thermodynamic calculations of $CeO_2$ stability under hydrothermal conditions reveal that at pH = 7, a pressure of 300 bars and under reductive conditions, $Ce^{3+}$ species ($CeO^+$, $CeOH^{2+}$, $Ce^{3+}$) start to dominate over $Ce^{4+}$ species upon cooling from 370 °C to 150 °C.[21] This is in phase with the rather low thermal stability of $CeCO_3OH$, which depends strongly on the conditions it is exposed to.[47] Under reductive ($H_2$) static gaseous conditions, decomposition starts at 248 °C until 455 °C to form $CeO_2$, with 75% of mass loss occurring before reaching 400 °C.[47] Note that under inert conditions, the range of the decomposition temperature of $CeCO_3OH$ increased to 336–467 °C. Based on these two facts, the hypothesis can be drawn that the formation of $CeCO_3OH$ observed after batch tests occurs upon cooling down at the end of the batch test. Indeed, during the cooling, $CeO_2$ is exposed to conditions that will favour the formation of the hydroxy carbonate, that is, $CO_2$ in excess, a temperature lower than 400 °C, and reducing conditions, thanks to the presence of unreacted glycerol and to its decomposition products such as $H_2$ and CO, but also acrolein, propionaldehyde, acetaldehyde and allyl alcohol.[48] The very different conditions $CeO_2$ is exposed to during the batch *vs.* continuous tests are displayed in Fig. 2. In this Figure, the lines represent the boundaries delimiting the conditions below which one or several aqueous $Ce^{3+}$ species are likely to be equilibrated

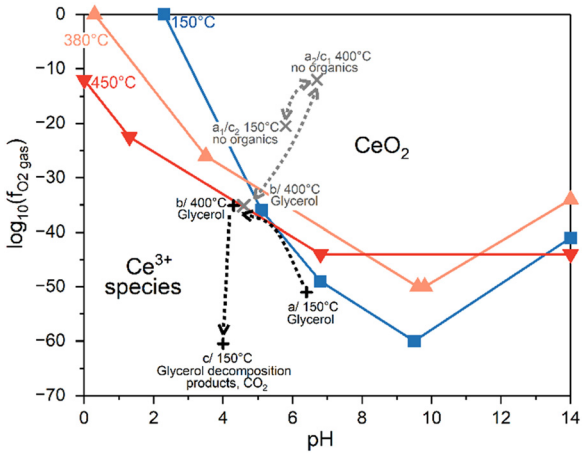


**Fig. 2** Calculated $f_{O_2}$ - pH diagrams for the Ce–$H_2O$ system. $f_{O_2}$ is expressed in bar, and pH is in $\log_{10}$(mol $kg^{-1}_{H_2O}$). Boundaries indicated for different temperature delimits the conditions below which one or several aqueous $Ce^{3+}$ species are likely to be equilibrated at a concentration higher than ≈1 μmol $kg^{-1}_{H_2O}$. Conditions applied during batch experiments are presented in black: a/step during heating up, b/ steady reaction, c/step during cooling. Conditions applied during continuous test are in grey: $a_1$/step during heating up, $a_2$/steady temperature, under pure water, b/steady reaction with glycerol, $c_1$/ flushing step with water, $c_2$/step during cooling. Adapted from.[21]

at a concentration higher than ≈1 μmol $kg^{-1}_{H_2O}$, for different temperatures. Above these lines, $CeO_2$ dominates and these water-soluble $Ce^{3+}$ species have concentrations below the ppm range. The black crosses, representing the conditions met during a batch test, clearly show that during all steps Ce reduction and the formation of water-soluble species were favoured. During a continuous test (grey points), the material would not be exposed to such unfavourable conditions, *i.e.* $CeO_2$ is expected to be stable. However, when glycerol is fed continuously, this limit is likely reached. Note that the effect of batch *vs.* continuous flow on the pH is complicated to assess, but a lower pH is expected during the batch test.

To test this hypothesis, experiments with pure $CeO_2$ oxide under continuous flow of a 10 wt% glycerol solution were performed at 430 °C, 270 bar and 15 g $min^{-1}$ for 3 h. After the experiment was completed, the catalyst bed was rinsed with water for 45 min (at SCW conditions), after which the system was cooled under water (typical steps followed for any continuous test) (see grey crosses in Fig. 2). In this case, a significantly smaller decrease in both BET surface area and pore volume was observed after the continuous SCWG of glycerol (20 $m^2$ $g^{-1}$ and 0.095 $cm^3$ $g^{-1}$), similar to the decrease observed after the batch test with pure SCW (27 $m^2$ $g^{-1}$and 0.095 $cm^3$ $g^{-1}$), and the crystallite size were found to be nearly identical, at 28 and 30 nm, respectively. Most importantly, the analysis of the material after the test revealed the total absence of $CeCO_3OH$ (Fig. 1). These observations are in line with the hypothesis that $CeCO_3OH$ formed predominantly upon quenching the batch reactor, as depicted in Fig. 2. Therefore, the primary reduction in the $S_{BET}$ of pristine $CeO_2$ (from 53 down to 20–27 $m^2$ $g^{-1}$) is probably due to the harsh environmental conditions of SCW. Further reduction of the surface area (from 20–27 down to 7.0 $m^2$ $g^{-1}$) is likely linked to the formation of large $CeCO_3OH$ crystals during the gasification of glycerol (only during batch experiments, when a solid sample remains in the reaction medium during cooling). These results, however, do not exclude the possibility that some $CeCO_3OH$ was formed during continuous flow reaction and then decomposed in the presence of pure water. The concentration of cerium ions found in the process water produced using 0.44%Ru/$CeO_2$_700 at 401 °C, 270 bar and a flow rate of 7.2 g $min^{-1}$ of 10 wt% glycerol was 4.6 × $10^{-8}$ $mol_{Ce}$ $kg^{-1}$, matching the values predicted by thermodynamic calculations.[21]

With the aim to increase the stability of the $CeO_2$ support (before SCWG experiment), the effect of stabilization of $CeO_2$ by thermal treatment at 500, 700, and 900 °C was investigated. The XRD patterns of the calcined powders show the expected behavior, with narrower and more intense peaks being observed as the calcination temperature increases (Fig. S4). Thus, the coherence length estimated *via* Rietveld refinement increased from 18 nm (for the unmodified sample) to 20, 31, and 82 nm after treatment at 500, 700, and 900 °C, respectively. Accordingly, specific surface area and total pore volume decrease due to particle coarsening (Table 2 and Fig. S5). For $CeO_2$ treated at 500 °C, no changes were observed with respect to pristine $CeO_2$ ($S_{BET}$ = 53 $m^2$ $g^{-1}$ and $V_{total}$ = 0.098 $cm^3$ $g^{-1}$), but after calcination at higher temperatures (700 and 900 °C), the $S_{BET}$ values dropped to 30 and 3.0 $m^2$ $g^{-1}$, and $V_{total}$ to 0.068 and 0.022 $cm^3$ $g^{-1}$, respectively.

As expected, the performed $CeO_2$ calcination proved to be beneficial to the stability of the catalyst in SCWG process. As shown in Table 2 and S3, increased calcination temperature decreased the loss in the specific surface area and pore volume

**Table 2** Evolution of surface area and total pore volume of pristine $CeO_2$ and after various thermal treatments and SCWG experiments

| Sample | $S_{BET}$ [$m^2$ $g^{-1}$] | $V_{total}$ [$cm^3$ $g^{-1}$] | $\Delta^{spent,a}_{fresh}$ ($S_{BET}$)[%] Batch[b]/continuous[c] SCWG | $\Delta^{spent,a}_{fresh}$ ($V_{tot}$)[%] |
|---|---|---|---|---|
| $CeO_2$[d] | 53 | 0.098 | −87/−62 | −71/−3 |
| $CeO_2$_500 | 30 | 0.098 | n.d. | n.d. |
| $CeO_2$_700 | 30 | 0.068 | n.d./−40 | n.d./−1 |
| $CeO_2$_900 | 3.0 | 0.022 | 0/−3 | 0/0 |

[a] Fresh and spent refer to the sample before and after the SCWG test, respectively. [b] Batch reaction conditions. [c] Continuous conditions. [d] As received $CeO_2$.

after SCWG experiments (more noticeable for $S_{BET}$ then $V_{total}$). For example, for $CeO_2$ annealed at the highest investigated temperature (900 °C) only minimal changes were observed ($S_{BET}$ = 3.0 $m^2$ $g^{-1}$ *vs.* 2.9 $m^2$ $g^{-1}$, while $V_{total}$ was identical in both cases, $V_{total}$ = 0.022 $cm^3$ $g^{-1}$). The higher structural stability of the material can be explained by the larger particles it is composed of, resulting in a much lower surface energy contribution to minimize *via* coarsening. It should be noted, however, that this stability is accompanied by a very low specific surface area, which is partially explained by the high density of $CeO_2$ (7.22 g $cm^{-3}$). Additionally, the high-temperature calcination process is associated with a much less pronounced formation of $CeCO_3OH$ phase under batch conditions (Fig. S6), which probably is mainly caused by the lower surface area of $CeO_2$ exposed to reactive conditions. Based on Rietveld's refinements (Fig. S2C), it was estimated that this sample consists of as much as 86 wt% $CeO_2$ and only 14 wt% $CeCO_3OH$ (which is more than a threefold decrease in the mass of $CeCO_3$-OH compared to the non-calcined $CeO_2$ sample).

### Ru/$CeO_2$ performance

The efficiency of Ru/$CeO_2$ catalysts (Ru loading 0.11, 0.25 and 1.00 wt%) in continuous SCWG of 3 wt% glycerol was studied at a pressure of 275 bar, 400–430 °C and weight hourly space velocities (WHSV) in the range of 1100–3400 $g_{glycerol}$ $g_{Ru}^{-1}$ $h^{-1}$. Film and internal mass transfer limitations were assessed using Mears' criterion and the Weisz–Prater criterion and were proven to be negligible (see details in SI). Since the considered materials differed significantly in Ru loading, their efficiency was expressed as the apparent carbon conversion rate ($r_{Xc}$), based on the TOC analysis of the process water, per gram of active phase (Ru) and per unit of time (h), Fig. S7 and Table 3. The 0.11%Ru/$CeO_2$_900 and 0.25%Ru/$CeO_2$_700 catalysts showed calculated $r_{Xc}$, averaged over the steady-state reached at specific conditions, ranging from *ca.* 470 ± 30 to 1290 ± 60 $g_C$ $g_{Ru}^{-1}$ $h^{-1}$ and from 430 ± 30 to 990 ± 50 $g_C$ $g_{Ru}^{-1}$ $h^{-1}$, respectively. Importantly, in both time intervals, in which the same conditions of the SCWG experiment occurred (400 °C, 10 g $min^{-1}$), the 0.11%Ru/$CeO_2$_900 catalyst showed a very high carbon conversion of 96 ± 3% and 98 ± 5% (Time On Stream (TOS) = 2.8 and 6.4 h, respectively), which resulted in almost identical apparent carbon conversion rates of 1270 ± 40 and 1290 ± 60 $g_C$ $g_{Ru}^{-1}$ $h^{-1}$. In turn, 0.25%Ru/$CeO_2$_700 tested under the same conditions exhibited a slightly lower conversion value, *i.e.* 78 ± 4% (TOS = 3.8 h) and 71 ± 3% (TOS = 6.2 h), which corresponded to 990 ± 50 and 910 ± 40 $g_C$ $g_{Ru}^{-1}$ $h^{-1}$, respectively. Therefore, it can be stated that both tested catalysts exhibit high stability indicated by good performance repeatability for changing SCWG conditions over time. Moreover, it should also be noted that for these catalysts, regardless of the reaction conditions, the C-based glycerol conversion always reached values above 70% (Table 3), therefore the calculated apparent conversion rate values were not determined in the kinetic regime. In contrast, the sample with the highest Ru loading (1.00 wt%) showed a much lower apparent conversion rate (*ca.* 220 ± 10 to 460 ± 10 $g_C$ $g_{Ru}^{-1}$ $h^{-1}$, depending on SCWG conditions) compared to the other tested Ru/$CeO_2$ catalysts with lower Ru content. However, despite the lower efficiency, it did not show any signs of deactivation in the tested timeframe, as for the catalysts with lower loading.

In turn, 0.44%Ru/$CeO_2$_700 was tested twice. The first measurement was performed at 400 °C, 275 bar pressure and varying feed glycerol concentrations (3, 6 and 10 wt%), Fig. S7D. At low glycerol content during the SCWG run (3 wt% glycerol, 7.5 g $min^{-1}$), the apparent carbon conversion rate was 780 ± 10 $g_C$ $g_{Ru}^{-1}$ $h^{-1}$, and after increasing the glycerol mass flow rate to 12.0 g $min^{-1}$, a value of 1260 ± 10 $g_C$ $g_{Ru}^{-1}$ $h^{-1}$ was achieved. A similar value (1310 ± 10 $g_C$ $g_{Ru}^{-1}$ $h^{-1}$) was noted after increasing the glycerol feed concentration to 6 wt% and at a mass flow rate of 7.5 g $min^{-1}$. However, further increasing the glycerol solution concentration to 10 wt%,

**Table 3** Conditions of continuous SCWG of 3 wt% glycerol and performance of Ru/$CeO_2$ catalysts

| Catalyst | TOS [h] | Temperature [°C] | Flow rate [g $min^{-1}$] | $WHSV_{Ru}$ [$g_{glycerol}$ $g_{Ru}^{-1}$ $h^{-1}$] | Conversion [%] | Apparent C conversion rate [$g_C$ $g_{Ru}^{-1}$ $h^{-1}$] |
|---|---|---|---|---|---|---|
| 0.11%Ru/$CeO_2$_900 | 1.0 | 401 | 7.2 | 2380 | 90 ± 1 | 840 ± 10 |
| | 2.8 | 401 | 10.3 | 3390 | 96 ± 3 | 1270 ± 40 |
| | 5.0 | 427 | 3.7 | 1220 | 98 ± 6 | 470 ± 30 |
| | 6.4 | 401 | 10.2 | 3370 | 98 ± 4 | 1290 ± 60 |
| 0.25%Ru/$CeO_2$_700 | 1.5 | 401 | 7.1 | 2260 | 89 ± 4 | 790 ± 30 |
| | 3.8 | 400 | 10.2 | 3270 | 78 ± 4 | 990 ± 50 |
| | 5.2 | 432 | 3.7 | 1170 | 93 ± 6 | 430 ± 30 |
| | 6.2 | 401 | 10.3 | 3290 | 71 ± 3 | 910 ± 40 |
| 0.44%Ru/$CeO_2$_700 | 1.5 | 400 | 7.5 | 2010 | 99 ± 1 | 780 ± 10 |
| | 2.9 | 400 | 12.0 | 3230 | 99 ± 1 | 1260 ± 10 |
| | 4.5 | 400 | 7.5 | 4060 | 83 ± 7 | 1310 ± 10 |
| | 6.0 | 400 | 7.5 | 6870 | 28 ± 6 | 740 ± 10 |
| 1.00%Ru/$CeO_2$_700 | 1.0 | 399 | 7.4 | 2270 | 52 ± 1 | 460 ± 10 |
| | 2.0 | 400 | 3.7 | 1140 | 50 ± 1 | 220 ± 10 |
| | 3.3 | 400 | 10.3 | 3180 | 35 ± 1 | 430 ± 10 |
| | 4.5 | 430 | 4.0 | 1230 | 57 ± 2 | 270 ± 10 |
| | 5.5 | 401 | 10.3 | 3160 | 34 ± 1 | 420 ± 10 |

while maintaining the feed mass flow rate, resulted in a significant drop in conversion (to 28 ± 1%), which was reflected in a decrease in the apparent conversion rate to 740 ± 10 $g_C$ $g_{Ru}^{-1}$ $h^{-1}$. The second measurement was performed under constant SCWG conditions (*i.e.*, 400 °C, 275 bar, 5 g $min^{-1}$, 3 wt% glycerol), to determine the stability of this catalyst over time on stream (Fig. S7E). Under the applied conditions, a noticeable decrease in the apparent carbon conversion rate was observed (from 2200 ± 60 to 1340 ± 20 $g_C$ $g_{Ru}^{-1}$ $h^{-1}$), indicating a similar degree of deactivation as that reported for CNF-supported Ru nanoparticles;[25,48] both points being further discussed in the next sections. Additionally, the apparent carbon conversion rate based on the gasification efficiency values ($r_{GEc}$) depicted in Fig. S8 showed similar numbers to those discussed in Fig. S7. However, the apparent deviations between the recorded points at each time interval were caused by the low gas flow and the dilution of the gas effluent by $N_2$ used to prevent GC detector peak saturation by $H_2$ as well as to increase the gas pressure for low gas production experiments.

For all tested $Ru/CeO_2$ catalysts, the main reaction products were $CO_2$, $CH_4$, and $H_2$. With the change of SCWG process conditions (and the extension of reaction time), the gas composition changed slightly. Over 0.11%$Ru/CeO_2$_900, the $H_2$ content in the produced gas increased from 17 ± 1 to 31 ± 2 vol% at the expense of $CH_4$, which decreased from 47 ± 3 to 38 ± 3 vol%. A similar decreasing trend of produced $CH_4$ was observed with 0.25%$Ru/CeO_2$_700 as well as 1.00%$Ru/CeO_2$_700 (drop from 33 ± 2 to 22 ± 2 vol% and from 28 ± 1 to 19 ± 2 vol%, respectively). During this time, the $H_2$ concentration in the gas mixture also changed, with a clearly visible upward trend (31 ± 2 to 42 ± 2 for 0.25%$Ru/CeO_2$_700 and 38 ± 2 to 44 ± 2 for 1.00%$Ru/CeO_2$_700). For all tested catalysts and SCWG conditions, the concentration of $CO_2$ produced remained at a similar level and ranged from 32 ± 2 to 38 ± 2 vol%, while the CO content was usually below 1 vol%.

Fig. 3 shows the apparent carbon conversion rate over $Ru/CeO_2$ samples (Ru loading: 0.11, 0.25 and 1.00 wt%) determined after 6 h of operation at a pressure of 275 bar, a temperature of 400 °C and a flow rate of 10 g $min^{-1}$ of 3 wt% glycerol in water. This comparison also included the results obtained under the same temperature and pressure but lower feed mass flow rate, *i.e.* 5 g $min^{-1}$ for 0.44%$Ru/CeO_2$_700 and 6 g $min^{-1}$ for the research benchmark 5.00%Ru/CNF catalyst, which showed the highest performance in our previous studies,[25] and the commercial benchmark 5.02%Ru/AC catalyst used at pilot scale.[49] Among the studied $Ru/CeO_2$ samples, the highest apparent carbon conversion rate was observed for 0.44%$Ru/CeO_2$_700 and 0.11%$Ru/CeO_2$_900, for which value of 1340 ± 20 and 1230 ± 60 $g_C$ $g_{Ru}^{-1}$ $h^{-1}$ were obtained, respectively. For other $CeO_2$-supported catalysts, lower apparent conversion rate values were achieved, *i.e.* 910 ± 40 $g_C$ $g_{Ru}^{-1}$ $h^{-1}$ for 0.25%$Ru/CeO_2$_700 and 420 ± 10 $g_C$ $g_{Ru}^{-1}$ $h^{-1}$ for 1.00%$Ru/CeO_2$_700.

For comparison, the commercially available 5.02%Ru/AC catalyst reached 510 ± 20 $g_C$ $g_{Ru}^{-1}$ $h^{-1}$, which is slightly higher

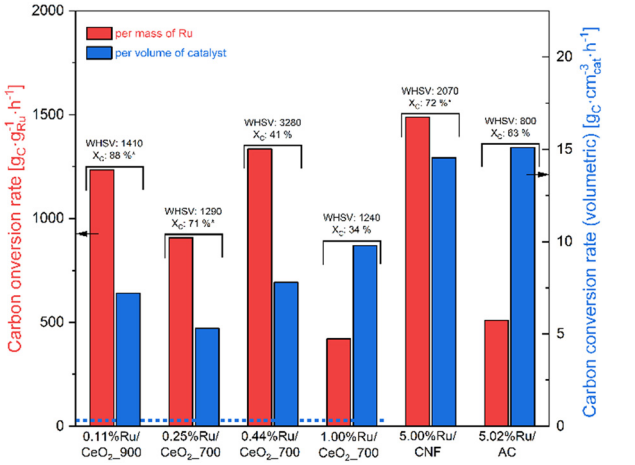


**Fig. 3** Apparent C conversion rate per gram of Ru (red bars) and per catalyst bed volume (blue bars). The dotted blue line indicates the volumetric conversion rate determined for $CeO_2$_700 support. Conditions of SCWG: 3 wt% glycerol in water, $p$ = 275 bar, $T$ = 400 °C, feed flow rate of 10 g $min^{-1}$ for 0.11%$Ru/CeO_2$_900, 0.25%$Ru/CeO_2$_700, 1.00%$Ru/CeO_2$_700 samples, 5 g $min^{-1}$ for 0.44%$Ru/CeO_2$_700 and 6 g $min^{-1}$ for 5.00%Ru/CNF and 5.02%Ru/AC. Apparent carbon conversion values and WHSV in $g_C$ $g_{Ru}^{-1}$ $h^{-1}$ are given in the figure. The asterisks indicate a possible apparent conversion rate underestimation because the conversion was not low enough.

than for 1.00%$Ru/CeO_2$_700, and at the same time almost two and three times lower than for 0.25%$Ru/CeO_2$_700 and 0.11%$Ru/CeO_2$_900 as well as 0.44%$Ru/CeO_2$_700, respectively, which clearly indicates the high efficiency of the investigated catalysts. In turn, the benchmark 5.00%Ru/CNF catalyst turned out to be only slightly more effective compared to $Ru/CeO_2$, achieving an apparent C conversion rate of 1490 ± 30 $g_C$ $g_{Ru}^{-1}$ $h^{-1}$. As the spent catalysts had different specific surface areas, the apparent carbon conversion rate was also calculated based on the measured BET values. Considering the $Ru/CeO_2$ systems, the highest value of 0.49 $g_C$ $m^{-2}$ $h^{-1}$ was achieved for 0.11%$Ru/CeO_2$_900, while for the other catalysts with higher Ru loading, 0.35 $g_C$ $m^{-2}$ $h^{-1}$ was reached for 0.44%$Ru/CeO_2$_700 and 1.00%$Ru/CeO_2$_700, and only 0.21 $g_C$ $m^{-2}$ $h^{-1}$ for 0.25%$Ru/CeO_2$_700. It is worth mentioning that in the case of pure $CeO_2$_700 support this value was only 0.02 $g_C$ $m^{-2}$ $h^{-1}$, which indicates that the influence of the $CeO_2$ matrix itself on the SCWG process is virtually insignificant. On the other hand, for carbon-supported catalysts these values were calculated to be 0.25 $g_C$ $m^{-2}$ $h^{-1}$ (5.00%Ru/CNF) and 0.31 $g_C$ $m^{-2}$ $h^{-1}$ (5.02%Ru/AC). Additionally, the tested supported catalysts possess also different bulk densities, which were determined by the tap density method. The dry catalyst was placed into a narrow glass tube, which was tapped until the catalyst bed volume did not change. The bulk density calculated in this way was 2.33 g $cm^{-3}$ for all $Ru/CeO_2$, while much lower values of 0.60 g $cm^{-3}$ and 0.20 g $cm^{-3}$ were noted for 5.02%Ru/AC and 5.00%Ru/CNF, respectively, which is inversely proportional to the volume of the catalyst bed in the reactor. At elevated pressure and temperature, reactor volume is costly; thus, reducing it, for example by employing high-density catalysts, can significantly

lower the capital expenditure of a cSCWG process. Therefore, the performance of the studied catalyst was calculated as an apparent conversion rate of glycerol per catalyst volume (Fig. 3, blue bars). Among the $CeO_2$ supported samples, the highest value of 9.8 $g_C$ $cm_{cat}^{-3}$ $h^{-1}$ is achieved with the 1.00%Ru/$CeO_2$_700 sample, which was previously considered to be the least promising when considering the apparent conversion rate per gram of Ru. The 0.44%Ru/$CeO_2$_700 and 0.11%Ru/$CeO_2$_900 performed slightly worse, reaching values of 7.8 and 7.2 $g_C$ $cm_{cat}^{-3}$ $h^{-1}$, respectively, while the weakest system turned out to be 0.25%Ru/$CeO_2$_700 with a value of 5.3 $g_C$ $cm_{cat}^{-3}$ $h^{-1}$. On the other hand, both reference catalysts exhibit the highest efficiency with values of 14.5 and 15.1 $g_C$ $cm_{cat}^{-3}$ $h^{-1}$ for 5.00%Ru/CNF and 5.02%Ru/AC, respectively.

Fig. 4 shows the relationship between gas composition and conversion of glycerol feed (3 wt%) achieved at 400 °C and 270 bar over Ru/$CeO_2$ and Ru/CNF catalysts. In both cases the main reaction products were $H_2$, $CO_2$, and $CH_4$, while CO was marginal. Both classes of catalysts performed very similarly over the range of apparent conversion rates tested. However, Ru/$CeO_2$ seems to slightly favour $CH_4$ production, while Ru/CNF slightly favours hydrogen production. For both types of catalysts and at conversions below 90%, the $H_2$ and $CH_4$ concentrations in the gas were in the range of 34–46 and 18–28 vol%, respectively. Interestingly, when conversion reaches a level above 90%, a noticeable increase in $CH_4$ production was observed at the expense of $H_2$. On the other hand, no influence of glycerol conversion and catalyst type on the amount of $CO_2$ (approx. 30–40 vol%) and CO (less than 1 vol%) produced was detected. In our previous research,[25,48] slightly higher $CH_4$ and lower $H_2$ concentrations were measured in the produced gas when Ru/CNF catalysts were used, which is directly linked to the different feed concentrations.[31,50]

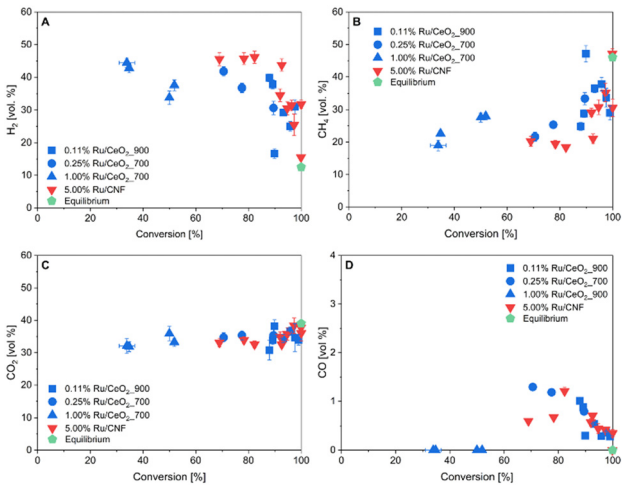


Fig. 4 Relationship between gas composition ($H_2$, $CH_4$, $CO_2$ and CO in A, B, C and D, respectively) and conversion of glycerol (3 wt%) achieved at 400 °C and 270 bar over Ru/$CeO_2$ and Ru/CNF catalysts.

SCWG experiments were also carried out using 10 wt% of glycerol, maintaining the pressure and temperature used previously (Fig. S9). Increasing the glycerol content in the feed resulted in a significant change in conversion, which significantly dropped with most points below 30 and 50% for both Ru/$CeO_2$ and Ru/CNF catalysts, respectively. This notably influenced the gas composition, with overall higher $H_2$ and lower $CH_4$ concentrations for the Ru/$CeO_2$ than for the Ru/CNF catalyst. However, there was a clear difference between the two catalysts, with a much higher $H_2$ concentration, a higher $CO_2$ and a lower $CH_4$ concentration for Ru/$CeO_2$ when compared with Ru/CNF. Surprisingly, CO levels were found to be very different between the two catalysts, with a concentration peaking at 25 vol% for Ru/CNF at 17% conversion, while for Ru/$CeO_2$ the CO concentration always remained very low. A similar behaviour was found for Ru/$CeO_2$ catalysts when changing from 3 to 10 wt% glycerol, while a comparison was not possible for Ru/CNF because of the lack of data at low conversion and 3 wt% glycerol. The different gas composition can be explained by an accelerated water gas shift (WGS) reaction over $CeO_2$, which oxidizes CO with water to produce $H_2$ and $CO_2$.

To recognise the influence of the $CeO_2$ support itself on the glycerol gasification process, experiments were carried out using Ru-free $CeO_2$_700 (Fig. S10A). This sample (previously calcined at 700 °C) showed a low carbon conversion of 12.2 ± 0.2% at a pressure of 275 bar, a temperature of 427 °C and a low feed flow rate of 3.7 g $min^{-1}$ of 3 wt % glycerol in water. When the temperature was lowered to 400°C and the feed mass flow rate was doubled (to 7.3 g $min^{-1}$), the conversion dropped by a factor of three, reaching just 3.2 ± 0.1%. However, this had no significant effect on the gas composition, where the main products in both cases were $H_2$ (approx. 50 vol%) and $CO_2$ (approx. 30 vol%). On the other hand, CO was in the range of 14–17 vol%, while $CH_4$ was only 1 vol%. No other gaseous products were observed. These observations, compared to data in Fig. 4, indicates that there is a synergy between Ru and $CeO_2$. Indeed, $CeO_2$ alone produces large amounts of CO but no $CH_4$ at low conversion, while with Ru/$CeO_2$, $CH_4$ formation is observed but no CO. Interestingly, for the same sample, but after an additional reduction step in $H_2$ under the same conditions as during the pretreatment of Ru/$CeO_2$ catalyst precursors, a lower carbon-based conversion of glycerol as well as a different composition of the produced gas were observed (Fig. S10B). In this case, the conversion was in the range of 5–8 ± 1%, depending on the SCWG process conditions. In terms of gas composition, apart from minor changes in the concentration of $H_2$, $CO_2$, and $CH_4$, the main difference was the detection of propane instead of CO. The cause of the selective production of propane, through successive dehydration and hydrogeneration, instead of CO cannot be explained with the information gathered. However, it can be stated that the different selectivity of both supports is clearly due to the different thermal pre-treatments of the $CeO_2$, which likely affected the reduction state of cerium oxide and the concentration of oxygen vacancies,[51] despite an exposure to air before loading the material in the reactor. $CeO_2$ participates in

the SCWG process, but its activity is negligible compared to Ru, and its selectivity depends on the pretreatment of the solid.

### Ru/$CeO_2$ evolution during SCWG

After the modification of the $CeO_2$ support by incipient wetness impregnation with the Ru precursor and subsequent thermal reduction with $H_2$ at 300 °C, no change in $CeO_2$ crystallinity was observed and no other additional phases were detected by XRD (Fig. S11A–D). The lack of a crystalline $Ru^0$ or any other ruthenium-based diffraction lines in the XRD patterns for all Ru/$CeO_2$ samples might be a result of the very low loading and/or the low size of Ru particles (less than a few nanometers). In the case of both reference catalysts, which contained a higher amount of Ru (5 wt%), also no Ru phase signals were observed, which may be related to the much higher porosity of these catalysts (Table 4). Since only a small amount of Ru was deposited on the $CeO_2$ surface, the catalysts showed a porosity comparable to the unmodified $CeO_2$ supports (Table 4). The 0.11%Ru/$CeO_2$_900 catalyst exhibited low $S_{BET}$ and $V_{total}$ values (3.0 $m^2$ $g^{-1}$ and 0.023 $cm^3$ $g^{-1}$, respectively), because of the low porosity of the support, calcined at 900 °C. All Ru/$CeO_2$ catalysts containing higher Ru loadings showed values close to the values for their support $CeO_2$_700. After the glycerol gasification experiments, the XRD patterns recorded for the Ru/$CeO_2$ samples remained unchanged and no characteristic reflections of the $CeCO_3OH$ phase were observed in any of the tests performed in the continuous setup (Fig. S11). Moreover, the average $CeO_2$ crystallite size evaluated *via* Rietveld refinement increased slightly for the spent catalysts (Table 4). For all higher Ru loading catalysts (0.25–1.00 wt%), the $V_{total}$ and $S_{BET}$ values decreased by about 25–35% and 50–60%, respectively, after SCWG tests. These changes suggest partial degradation of the catalysts, probably due to coarsening of $CeO_2$ ("sintering") and/or blocking of existing pores, *e.g.* by recrystallization under SCW/SCWG conditions. In turn, such a reduction of both parameters was neither observed for 0.11%Ru/$CeO_2$_900 nor for $CeO_2$_900. For both reference catalysts, an increase in $S_{BET}$ and $V_{total}$ values was observed after the SCWG experiment, which is consistent with the literature[20] and is related to the leaching and/or gasification of the least stable carbon present in the supports.

Importantly, these changes did not result in a loss of activity during the gasification process (Fig. S7 and S8), which indicate either that they have no impact in the total surface of active ruthenium, or that such loss occurred before the SCWG experiments. To confirm this hypothesis, a stability test was performed in only SCW to study its effect on surface area and pore volume. Indeed, already after 1 h under SCW conditions (275 bar, 430 °C), the BET specific surface area of 0.25% Ru/$CeO_2$_700 decreased from 28 to 16 $m^2$ $g^{-1}$, while the total pore volume remained almost unchanged (0.064 $cm^3$ $g^{-1}$ before and 0.065 $cm^3$ $g^{-1}$ after experiment). This result confirms that the loss of surface area of the catalyst during the test mostly occurs during the heating up and stabilisation phase in pure water flow. Note that there is a lack of consistency between the crystallite size and the BET surface area, for example between 1.00%Ru/$CeO_2$_700 and 1.00%Ru/$CeO_2$_700_S for which $S_{BET}$ decreased threefold but the crystallite size did not change (Table 4 and S4). This can be explained by coarsening leading do a decrease of the intercrystallite voids (aggregation of crystals to a large pore-free particle), without crystallite coalescence (two crystals fusing to a larger one). Another explanation would be the filling of intercrystallite voids with amorphous material which do not present diffuse scattering peaks in XRD.

**Table 4** Evolution of specific surface area, pore volume and crystallite size of $CeO_2$ in Ru/$CeO_2$ catalysts before and after (marked "_S") continuous SCWG of glycerol

| Sample | $S_{BET}$ [$m^2$ $g^{-1}$] | $V_{total}$ [$cm^3$ $g^{-1}$] | Crystallite size[a] [nm] |
|---|---|---|---|
| $CeO_2$_900 | 3.0 | 0.022 | 82 |
| 0.11%Ru/$CeO_2$_900 | 3.0 | 0.023 | 91 |
| 0.11%Ru/$CeO_2$_900_S | 2.9 | 0.022 | 94 |
| $CeO_2$_700 | 30 | 0.068 | 31 |
| $CeO_2$_700_S | 18 | 0.067 | 29 |
| 0.25%Ru/$CeO_2$_700 | 28 | 0.064 | 30 |
| 0.25%Ru/$CeO_2$_700_S | 11 | 0.042 | 36 |
| 0.25%Ru/$CeO_2$_700_SCW[b] | 16 | 0.065 | 34 |
| 0.44%Ru/$CeO_2$_700 | 34 | 0.078 | 26 |
| 0.44%Ru/$CeO_2$_700_S | 17 | 0.060 | 30 |
| 1.00%Ru/$CeO_2$_700 | 31 | 0.068 | 26 |
| 1.00%Ru/$CeO_2$_700_S | 12 | 0.045 | 26 |
| 5.00%Ru/CNF | 255 | 1.93 | n/a. |
| 5.00%Ru/CNF_S | 292 | 2.15 | n/a |
| 5.02%Ru/AC | 796 | 0.30 | n/a |
| 5.02%Ru/AC_S | 837 | 0.32 | n/a |

[a] Crystallite size of $CeO_2$ evaluated *via* Rietveld refinement. See Table S4 for comparison with data from the Scherrer equation. [b] Test performed in batch experiment with pure water for 1 h at 270 bar, 430 °C, to mimic the conditions the catalyst is exposed to prior to the start of a continuous test; n/a = not applicable.

 

The incipient wetness impregnation technique enables the deposition of very fine Ru particles on the support surface, as we have shown in our previous study on Ru/CNF.[25] In the case of this class of materials, Ru nanoparticles could be clearly identified, because of the high contrast compared to the CNF matrix. However, in the case of the discussed $Ru/CeO_2$ samples, the very low contrast between Ru nanoparticles ($Ru^0$ core with a $RuO_2$ shell),[52] makes the evaluation of Ru particle size distribution unrealistic by electron microscopy, as EDX analysis would be necessary to confirm the composition of each observed nanoparticles. TEM revealed first highly crystalline $CeO_2$ particles with a size in the same range as listed in Table 4, and with a low-porosity consisting of cavities in the 1–5 nm diameter range. As it can be seen in Fig. 5, pure $CeO_2$ showed 1–4 nm particles that could be observed at the edge of $CeO_2$ crystals on 0.44%$Ru/CeO_2$_700_S, as well as on Ru-free $CeO_2$_700_S. STEM-EDX analysis on several particles proved that most were $CeO_2$, but also a few were Ru nanoparticles. Additionally, the occurrence of these darker spots (potential Ru nanoparticles) is highly dependent on the appropriate focusing during the TEM measurement (Fig. S12). Therefore, for $Ru/CeO_2$ (regardless of the Ru loading) it is not possible to precisely identify Ru particles, and consequently their size and dispersion cannot be determined in a statistically meaningful way. Nevertheless, it should be emphasized that the identified particles (which can be assigned to both Ru- and $CeO_2$-based species) in the $Ru/CeO_2$ systems are in the range of 1.0 ± 0.2 to 1.6 ± 0.4 nm (Table S5). As a result of glycerol gasification, the size of these particles increased to values of 1.8 ± 0.5–2.5 ± 0.5 nm. A similar increase in Ru particle size after SCWG experiments was also observed for the reference 5.00% Ru/CNF catalyst used in this study (from 2.0 ± 0.6 to 3.1 ± 0.8 nm), and is also consistent with our previous findings, where stabilization in the range of 2.2–2.8 nm was observed in Ru/CNF catalysts (Ru loading range 1–30 wt%).[20,25] Interestingly, after 1 h of exposure of the 0.25%Ru/$CeO_2$_700 sample solely to SCW conditions (270 bar, 430 °C), the identified particles (which still can be assigned to both Ru- and $CeO_2$-based species) increased only slightly from 1.6 ± 0.4 to 1.7 ± 0.4 nm. It should be emphasized that the same observation (of lack of Ru particle size growth in pure SCW) was also confirmed in the case of Ru/CNF.[25]

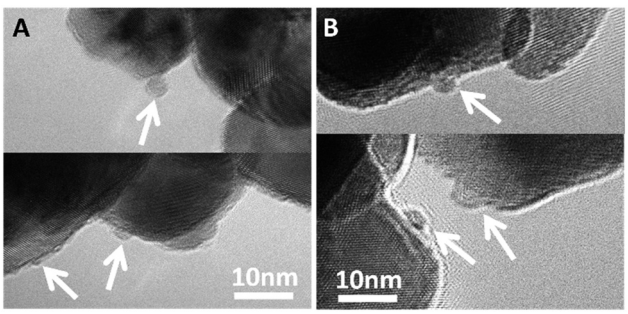


Fig. 5 HR-TEM images of the $CeO_2$_700_S support (A) and 0.44%Ru/$CeO_2$_700_S catalyst (B).

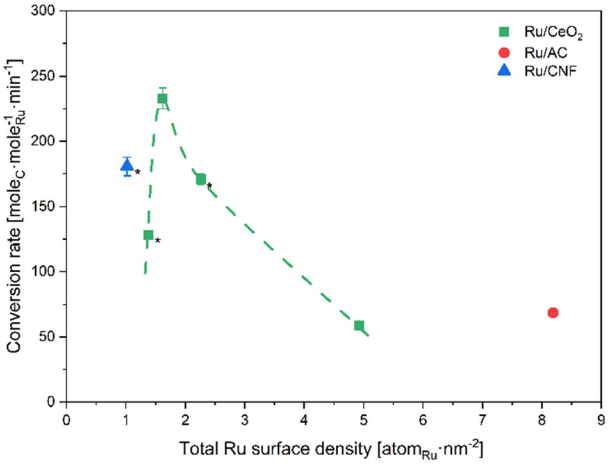


Fig. 6 Apparent carbon conversion rate over $Ru/CeO_2$, Ru/CNF and Ru/AC catalysts as a function of the total surface density of Ru. The asterisks (*) indicate a possible underestimation of the apparent conversion rate because the conversion was not low enough (<60%).

In our previous study with Ru/CNF, no correlation was found between Ru particle size and catalysts activity, however, a clear correlation was observed between the TOF and the surface density of active ruthenium on the catalyst surface.[25] Since the Ru dispersion could not be determined and thus the TOF value not calculated reliably in this study, the catalyst activity was expressed as the apparent carbon conversion rate as a function of total Ru surface density (Fig. 6). In this comparison, $Ru/CeO_2$ catalysts with 0.11–0.44 wt% Ru were the most efficient, achieving high apparent conversion rates (128–233 $mol_C$ $mol_{Ru}^{-1}$ $min^{-1}$), with a total Ru surface density of 1.4–2.3 $atom_{Ru}$ $nm^{-2}$ (maximum apparent conversion rate reached at 1.6 $atom_{Ru}$ $nm^{-2}$). In turn, for 1.00%$Ru/CeO_2$_700, the lowest conversion factor was recorded, which was only 59 $mol_C$ $mol_{Ru}^{-1}$ $min^{-1}$, which was accompanied by a high value for the total Ru density equal to 4.9 $atom_{Ru}$ $nm^{-2}$. Interestingly, both reference carbon-supported catalysts also follow this trend, as high activity was achieved for 5.00%Ru/CNF (181 $mol_C$ $mol_{Ru}^{-1}$ $min^{-1}$ at 1.0 $atom_{Ru}$ $nm^{-2}$), while 5.02%Ru/AC was characterized by a much lower efficiency (69 $mol_C$ $mol_{Ru}^{-1}$ $min^{-1}$), which was related to the high Ru density (7.2 $atom_{Ru}$ $nm^{-2}$).

While the exact origin of the performance decrease with increasing Ru loading remains unclear, two plausible explanations can be proposed: 1. an optimal balance between Ru active sites and the carbon support surface might exist, as the carbon support itself has demonstrated intrinsic activity in the hydrothermal conversion of organic compounds;[20,53] 2. for Ru particles supported on carbon a mild particle growth was reported under reductive supercritical water conditions,[25] and a similar particle size growth can be expected with $CeO_2$ support. Although the mechanism responsible for this growth is not fully understood, atomic migration–coalescence (Ostwald ripening) —*via* detachment and surface diffusion of Ru atoms on the support—may be involved. At higher Ru loadings, the increased surface density of Ru atoms would statistically reduce the fraction of isolated or low coordination Ru surface species. As

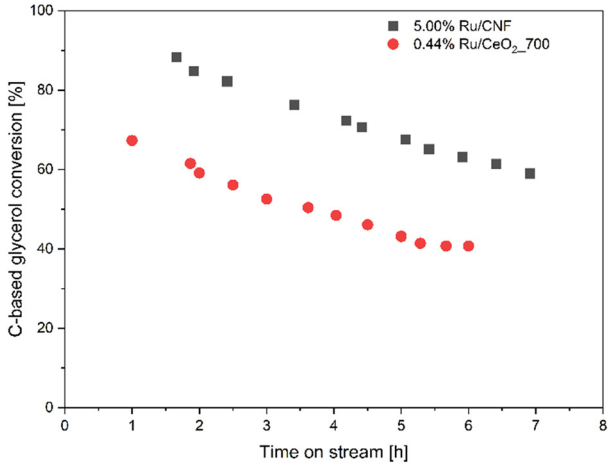


Fig. 7 Evolution of carbon (glycerol) conversion over 0.44%Ru/$CeO_2$_700 and 5.00%Ru/CNF and as a function of time on stream.

these sites have been suggested to exhibit particularly high intrinsic activity,[25] an increase in Ru loading could therefore lead to a lower overall catalytic efficiency due to a decreased proportion of highly active sites.

Literature reports consistently show that $CeO_2$ exhibits negligible acidity and only very weak basicity associated with surface hydroxyl groups.[54,55] $CO_2$-TPD and $NH_3$-TPD profiles of $CeO_2$ and Ru/$CeO_2$ remain essentially unchanged upon Ru addition, indicating that variations in Ru loading do not affect the acid–base characteristics of the support, particularly at loadings below 1 wt%. Therefore, differences in catalytic performance with Ru loading cannot be attributed to changes in acidity or basicity of $CeO_2$.

### Ru/$CeO_2$ evolution during SCWG

We have previously shown that the loss of activity of Ru/AC catalysts during SCWG is not related to leaching of Ru,[56] while catalyst coking as well as the decrease of dispersion of the active phase may be the main mechanism of its rapid deactivation. To determine the stability of the catalysts over time on stream, the 5.00%Ru/CNF and 0.44%Ru/$CeO_2$_700 samples were selected and subjected to the experiment under constant SCWG conditions (400 °C, 270 bar and WHSV equal to 5400 ± 100 $g_{glycerol}$ $g_{Ru}^{-1}$ $h^{-1}$ for 5.00% Ru/CNF, and 7200 ± 600 $g_{glycerol}$ $g_{Ru}^{-1}$ $h^{-1}$ for 0.44% Ru/$CeO_2$_700). In both cases, a similar decreasing trend in C-based glycerol conversion was observed during the SCWG experiment (Fig. 7). By extrapolation, the decrease in conversion expected after hundreds of hours on stream is around 46 and 49%, respectively (Fig. S13).

One of the factors responsible for the decrease in efficiency of both types of catalysts may be the increase in Ru particle size, which however cannot be reliably determined by TEM/STEM. On the other hand, it is also well known that catalysts undergo coking, which is one of the factors negatively affecting their performance in the SCWG process. Therefore, TGA-MS analysis was performed for all spent Ru/$CeO_2$ samples to determine the amount of possible coke deposits (Fig. S14). Additionally, fresh catalysts and the corresponding supports ($CeO_2$_700 and $CeO_2$_900) were analysed under the same conditions (Fig. S15). Fresh Ru-containing samples (previously reduced at 300 °C) show high thermal stability, as confirmed by the insignificant mass change (usually less than 0.6 wt%, a higher value was noted only for 0.44%Ru/$CeO_2$_700) recorded in the temperature range from 110 to 1000 °C (Table 5). Comparable mass decreases were also detected for pure $CeO_2$ samples, confirming that the mass decrease of fresh Ru/$CeO_2$ catalysts are related to the changes occurring in the $CeO_2$ matrix, which can be attributed to the desorption of chemically adsorbed oxygen, surface carbonates and/or desorption of surface lattice oxygen atoms.[57] In turn, a different behaviour was observed for the spent catalysts. For the 0.25%Ru/$CeO_2$_700_S and 1.00%Ru/$CeO_2$_700_S samples, the largest mass loss was observed with 4.01 and 3.83 wt%, respectively, with a sharp decrease at a temperature of about 300 °C. This was accompanied by the release of a large amount of $CO_2$

Table 5 Mass loss during TGA measurements and determined amount of carbon deposit in Ru/$CeO_2$ samples. n.d. = not detected, due to the difference between fresh and spent materials

| Sample | Mass loss [wt%] 110–400 °C | 110–1000 °C | Coke deposit after SCWG[a] [$mg_C$ $g_{cat}^{-1}$] |
|---|---|---|---|
| $CeO_2$_700 | 0.27 | 0.41 | — |
| $CeO_2$_700_S | 0.26 | 0.43 | — |
| $CeO_2$_900 | 0.04 | 0.07 | — |
| 0.11%Ru/$CeO_2$_900 | 0.04 | 0.10 | — |
| 0.11%Ru/$CeO_2$_900_S[b] | 0.03 | 0.09 | n.d. |
| 0.25%Ru/$CeO_2$_700 | 0.25 | 0.42 | — |
| 0.25%Ru/$CeO_2$_700_S | 3.62 | 4.01 | 33.7 |
| 0.44%Ru/$CeO_2$_700 | 0.63 | 0.93 | — |
| 0.44%Ru/$CeO_2$_700_S[b] | 0.86 | 1.16 | 2.3 |
| 1.00%Ru/$CeO_2$_700 | 0.36 | 0.56 | — |
| 1.00%Ru/$CeO_2$_700_S | 3.45 | 3.83 | 30.8 |

[a] Based on the mass difference between the fresh and spent sample in the range of 110–400 °C. [b] These samples were analysed twice with consistent results.

(mass line $m/z$ = 44), which clearly proves that at this temperature the coke deposited on the catalysts during the SCWG experiment was oxidized. If one considers the temperature range up to 400 °C ($CO_2$ release occurs below this temperature) as well as the slight mass changes in the corresponding fresh catalysts, 33.7 and 30.8 mg coke per 1 g of spent catalyst ($mg_C\ g_{cat}^{-1}$) can be estimated, respectively. Much less coke was found on 0.44%Ru/$CeO_2$_700_S, which amounted to only 2.3 $mg_C\ g_{cat}^{-1}$ corresponding to 0.23 wt% loss. In turn, the spent sample containing the lowest amount of Ru (0.11%Ru/$CeO_2$_900_S) did not show any mass change, which indicates negligible carbon deposits on this sample. Insignificant carbon deposits were also measured for the spent Ru-free $CeO_2$ sample ($CeO_2$_700_S). The comparison does not reveal a clear correlation between Ru loading and the extent of coking, and the reasons why certain samples exhibit higher coke deposition than others remain unclear.

In the case of carbon-based catalysts (*e.g.* Ru/AC, Ru/CNF), it is not possible to efficiently regenerate them by simple selective oxidation of the carbon deposits at elevated temperature, which is one of the main disadvantages of such systems. Conversely, this regeneration strategy can be readily implemented for Ru/$CeO_2$ systems, which represents a clear advantage of these catalysts. Additionally, in this work we have evaluated the possibility of catalyst bed regeneration using $H_2O_2$ as a mild oxidant at a moderate temperature of 110 °C, already applied to regenerate Ru/AC catalyst poisoned by sulfur.[26] A spent sample containing 0.44 wt% Ru was selected and treated with 5 wt% $H_2O_2$ solution for this study. The collected results presented in Fig. 8 clearly confirm the efficiency of the proposed method to remove coke, which neither showed any weight loss associated with carbon residue oxidation at temperature around 300 °C nor related $CO_2$ emission in the regenerated sample (0.44%Ru/$CeO_2$_700_R). It is worth emphasizing that the proposed regeneration technique can be used directly in the high-pressure reactor, without the need to remove the catalyst. Moreover, such treatment does not negatively affect the physicochemical properties of the recovered sample which is confirmed by XRD technique and $N_2$ adsorption.

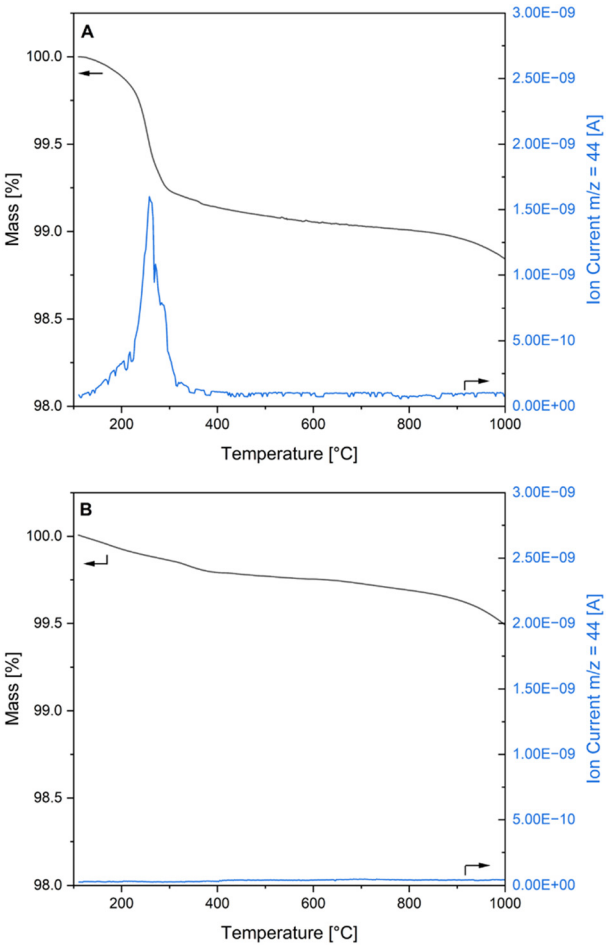


**Fig. 8** TGA profiles (black line) and $m/z$ = 44 MS line assigned to $CO_2$ (blue line) for spent 0.44%Ru/$CeO_2$_700_S catalyst (A) and after regeneration with $H_2O_2$ solution at 110°C (B).

## Conclusions

Overall, this study shows that $CeO_2$ is a promising non-carbon support for Ru in cSCWG, combining high activity, stability under optimized conditions, and practical regenerability – features that make it a strong candidate for industrial-scale biomass conversion.

$CeO_2$ undergoes transformation to $CeCO_3OH$ under hydrothermal batch conditions, causing surface area loss, but remains stable in continuous SCW provided pH > 6 and $CO_2$ exposure below 400 °C is avoided. Stability can be improved by pre-coarsening, with optimal calcination between 700–900 °C. Ru/$CeO_2$ catalysts exhibited excellent performance in cSCWG of glycerol at 400 °C and 270 bar, reaching conversion rates up to three times higher than commercial Ru/AC while showing similar selectivity trends. An optimal Ru surface loading of 1.5–2.0 $atom_{Ru}\ nm^{-2}$ was identified, slightly higher than on CNF-supported catalysts. A key advantage is the ease of coke and sulfur removal *via* mild oxidative treatments ($O_2$/air or $H_2O_2$), enabling efficient regeneration and lowering process costs. Future work should focus on elucidating the influence of catalyst preparation on coking behaviour and on optimizing regeneration protocols to ensure complete recovery of catalytic performance. From an industrial perspective, higher Ru loading is preferred as it reduces CAPEX linked to the costly volume of high-pressure, high-temperature reactors. However, this should not be at the cost of a much lower intrinsic activity of costly ruthenium. This underlines the importance of developing $CeO_2$-supported catalysts with stable and high surface area, enabling high Ru surface loading and improved volumetric catalytic performance for cSCWG. This could be reached, for example, by doping $CeO_2$, *e.g.* with Zr or Y, to improve the hydrothermal stability of the high surface area inorganic oxide.

## Author contributions

T. Kondratowicz: conceptualization, investigation, visualization, writing – original draft, writing – review and editing; A. Quenet: conceptualization, investigation, visualization, writing – original draft, writing – review and editing; X. Li: investigation, writing – review and editing; A. Testino: writing – review and editing; O. Kröcher: supervision, writing – review and editing; F. Vogel: conceptualization, funding acquisition, writing – review and editing; D. Baudouin: supervision, conceptualization, funding acquisition, visualization, writing – review and editing.

## Conflicts of interest

A. Quenet, F. Vogel and D. Baudouin declare that a patent application has been filed related to the technology described in this manuscript.

## Data availability

Data for this article, including raw experimental data and raw analytical files (TGA, $N_2$ adsorption, XRD, TEM) are available on Zenodo. See DOI: https://doi.org/10.5281/zenodo.20398121.

Supplementary information (SI) is available. See DOI: https://doi.org/10.1039/d5cy01486g.

## Acknowledgements

The authors acknowledge the financial support of BIOCTANE project with Grant No. 101084336 funded by the European Union. The authors would also like to thank Canio Scarfiello for the laboratory work on $CeO_2$ stability, Inge Stockinger as well as Patricia Pizarro de Oro and Sinay Sibaneth Turriziani (Rey Juan Carlos University) for performing the ICP-OES measurements, Songlan Sun for helping with the regeneration of the spent catalyst, Elisabeth Agnes Müller Gubler, Ivo Alxneit and Emiliya Poghosyan for their support with electron microscopy, Amel Tumbul, Norbert Schmid and Thomas Brunner for their support with the continuous test rig Konti-I.

## Notes and references

1 K. L. Ebi, J. Vanos, J. W. Baldwin, J. E. Bell, D. M. Hondula, N. A. Errett, K. Hayes, C. E. Reid, S. Saha, J. Spector and P. Berry, *Annu. Rev. Public Health*, 2021, **42**, 293–315.
2 K. Abbass, M. Z. Qasim, H. Song, M. Murshed, H. Mahmood and I. Younis, *Environ. Sci. Pollut. Res.*, 2022, **29**, 42539–42559.
3 The Paris Agreement | UNFCCC, https://unfccc.int/process-and-meetings/the-paris-agreement, (accessed May 9, 2025).
4 F. Gale, D. Goodwin, H. Lovell, H. Murphy-Gregory, K. Beasy and M. Schoen, *Int. J. Hydrogen Energy*, 2024, **59**, 654–667.
5 M. R. Errera, T. A. da C. Dias, D. M. Y. Maya and E. E. S. Lora, *Biomass Bioenergy*, 2023, **170**, 106721.
6 W. de Jong and J. R. van Ommen, in *Biomass as a sustainable energy source for the future: fundamentals of conversion processes*, ed. W. de Jong and J. R. van Ommen, Wiley, Hoboken, New Jersey, 2014, ch. III.
7 J. Giuntoli, *PhD thesis*, TU Delft, 2010.
8 A. A. Peterson, F. Vogel, R. P. Lachance, M. Froling, M. J. Antal and J. W. Tester, *Energy Environ. Sci.*, 2008, **1**, 32.
9 F. Vogel, in *Encyclopedia of Sustainability Science and Technology*, ed. R. Meyers, Springer, New York, 2017, pp. 1251–1295.
10 F. Vogel, Volume 2: Heterogeneous Catalysis, in *Handbook of Green Chemistry*, ed. R. H. Crabtree, Wiley, Weinheim, 2010, pp. 281–324.
11 N. Boukis, E. Hauer, S. Herbig, J. Sauer and F. Vogel, *Biomass Convers. Biorefin.*, 2017, **7**, 415–424.
12 D. C. Elliott, *Biofuels, Bioprod. Biorefin.*, 2008, **2**, 254–265.
13 B. Pinkard, J. Kramlich, P. Reinhall and I. Novosselov, in *Advanced Supercritical Fluids Technologies*, ed. I. Pioro, IntechOpen, 2019.
14 R. Muhlke, J.-B. Castaing, M. Morel and V. Donat, *Hydrothermal gasification - White paper*, GRTgaz, Bois-Colombes, France, 2023.
15 M. Schubert, J. W. Regler and F. Vogel, *J. Supercrit. Fluids*, 2010, **52**, 99–112.
16 P. A. Marrone, M. Hodes, K. A. Smith and J. W. Tester, *J. Supercrit. Fluids*, 2004, **29**, 289–312.
17 J. Reimer, G. Peng, S. Viereck, E. De Boni, J. Breinl and F. Vogel, *J. Supercrit. Fluids*, 2016, **117**, 113–121.
18 G. J. DiLeo and P. E. Savage, *J. Supercrit. Fluids*, 2006, **39**, 228–232.
19 E. Galiwango, J. Butler and S. Lotfi, *Fuels*, 2024, **5**, 375–393.
20 C. M. Hunston, *PhD thesis*, EPFL, 2021.
21 J. N. Jocz, P. E. Savage and L. T. Thompson, *Ind. Eng. Chem. Res.*, 2018, **57**, 8655–8663.
22 J. N. Jocz, L. T. Thompson and P. E. Savage, *Chem. Mater.*, 2018, **30**, 1218–1229.
23 S. Li, P. E. Savage and L. Guo, *J. Supercrit. Fluids*, 2018, **135**, 188–197.
24 J. G. Dickinson and P. E. Savage, *J. Mol. Catal. A: Chem.*, 2014, **388–389**, 56–65.
25 C. Hunston, D. Baudouin, L. Koning, A. Agarwal, O. Kröcher and F. Vogel, *Appl. Catal., A*, 2023, **320**, 121956.
26 M. Dreher, M. Steib, M. Nachtegaal, J. Wambach and F. Vogel, *ChemCatChem*, 2014, **6**, 626–633.
27 M. Dreher, B. Johnson, A. A. Peterson, M. Nachtegaal, J. Wambach and F. Vogel, *J. Catal.*, 2013, **301**, 38–45.
28 M. H. Waldner, *PhD thesis*, ETH Zurich, 2007.
29 TreaTech, personal communication, May 2025.
30 G. Peng, C. Ludwig and F. Vogel, *ChemCatChem*, 2016, **8**, 139–141.
31 H. Zöhrer, F. Mayr and F. Vogel, *Energy Fuels*, 2013, **27**, 4739–4747.
32 A. Abdulrasheed, A. A. Jalil, Y. Gambo, M. Ibrahim, H. U. Hambali and M. Y. Shahul Hamid, *Renewable Sustainable Energy Rev.*, 2019, **108**, 175–193.
33 P. Li, X. Chen, Y. Li and J. W. Schwank, *Catal. Today*, 2019, **327**, 90–115.

34 E. Aneggi, C. de Leitenburg, G. Dolcetti and A. Trovarelli, *Catal. Today*, 2006, **114**, 40–47.
35 C. de Leitenburg, A. Trovarelli, J. Llorca, F. Cavani and G. Bini, *Appl. Catal., A*, 1996, **139**, 161–173.
36 J. Liu, Z. Zhao, C. Xu and J. Liu, *Chin. J. Catal.*, 2019, **40**, 1438–1487.
37 K. Yuan, X.-C. Sun, H.-J. Yin, L. Zhou, H.-C. Liu, C.-H. Yan and Y.-W. Zhang, *J. Energy Chem.*, 2022, **67**, 241–249.
38 B.-S. Cheon, H.-M. Kim, J.-H. Hwang and D.-W. Jeong, *Fuel*, 2025, **383**, 133777.
39 C. Alvarez-Galvan, P. G. Lustemberg, F. E. Oropeza, B. Bachiller-Baeza, M. Dapena Ospina, M. Herranz, J. Cebollada, L. Collado, J. M. Campos-Martin, V. A. de la Peña-O'Shea, J. A. Alonso and M. V. Ganduglia-Pirovano, *ACS Appl. Mater. Interfaces*, 2022, **14**, 50739–50750.
40 R. Kopelent, A. Tereshchenko, A. Guda, G. Smolentsev, L. Artiglia, V. L. Sushkevich, A. Bugaev, I. I. Sadykov, T. Baidya, M. Bodnarchuk, J. A. van Bokhoven, M. Nachtegaal and O. V. Safonova, *ACS Catal.*, 2021, **11**, 9435–9449.
41 A. Solís-García, K. Portillo-Cortez, D. Domínguez, S. Fuentes-Moyado, J. N. Díaz de León, T. A. Zepeda and U. Caudillo-Flores, *Catalysts*, 2025, **15**, 301.
42 F. Cao, Y. Xiao, Z. Zhang, J. Li, Z. Xia, X. Hu, Y. Ma and Y. Qu, *J. Catal.*, 2022, **414**, 25–32.
43 D. Baudouin, H. Xiang and F. Vogel, *Biomass Bioenergy*, 2022, **164**, 106529.
44 Q. Guan, X. Huang, J. Liu, J. Gu, R. Miao, Q. Chen and P. Ning, *Chem. Eng. J.*, 2016, **283**, 358–365.
45 L. He, Y. Ren, Y. Fu, B. Yue, S. C. E. Tsang and H. He, *Molecules*, 2019, **24**, 526.
46 K. Michiba, R. Miyawaki, T. Minakawa, Y. Terada, I. Nakai and S. Matsubara, *J. Mineral. Petrol. Sci.*, 2013, **108**(6), 326–334.
47 X. Mao, X. Xia, J. Li, C. Chen, X. Gu, S. Li and Y.-P. Lan, *J. Alloys Compd.*, 2021, **870**, 159424.
48 D. Salionov, C. Hunston, F. Vogel, D. Baudouin and S. Bjelić, *J. Catal.*, 2023, **426**, 257–269.
49 F. Vogel, T. Brunner, D. Baudouin, R. Zambrano, G. Peng, A. Mian and M. Brandenberger, *Pilotanlage zur katalytischen hydrothermalen Vergasung nasser Biomasse - HydroPilot Pilot plant for the catalytic hydrothermal gasification of wet biomass*, SFOE, Villigen, Switzerland, 2023.
50 D. J. M. de Vlieger, A. G. Chakinala, L. Lefferts, S. R. A. Kersten, K. Seshan and D. W. F. Brilman, *Appl. Catal., A*, 2012, **111–112**, 536–544.
51 G. Feng, W. Han, Z. Wang, F. Li and W. Xue, *Catalysts*, 2018, **8**, 535.
52 R. Coloma Ribera, R. W. E. van de Kruijs, S. Kokke, E. Zoethout, A. E. Yakshin and F. Bijkerk, *Appl. Phys. Lett.*, 2014, **105**, 131601.
53 Y. Matsumura, Y. Suganuma, T. Ichikawa, W. Kim, Y. Nakashimada and K. Nishida, *ACS Omega*, 2021, **6**(36), 23442–23446.
54 Y. Zhao, C. Xi, S. Gao, Y. Wang, H. Wang, P. Sun and Z. Wu, *RSC Adv.*, 2023, **13**, 7037–7044.
55 N. Elia, J. Estephane, C. Poupin, B. El Khoury, L. Pirault-Roy, S. Aouad and E. A. Aad, *ChemCatChem*, 2021, **13**, 1559–1567.
56 C. Hunston, D. Baudouin, M. Tarik, O. Kröcher and F. Vogel, *Catal. Sci. Technol.*, 2021, **11**, 7431–7444.
57 N. H. T. Phan, C. C. Nguyen and M. T. N. Dinh, *RSC Adv.*, 2023, **13**, 13354–13364.